Advances in Atmospheric Sciences
Impact Factor: 5.8
E-alert
ISSN 0256-1530
CN 11-1925/O4

Weakening of Bomb Cyclones over the North Pacific in the Early 21st Century

Jiaxiang GAO, Rong-Hua ZHANG, Hai ZHI

Citation: Gao, J. X., R.-H. Zhang, and H. Zhi 2025: Weakening of Bomb Cyclones over the North Pacific in the Early 21st Century, *Adv. Atmos. Sci.*, 42, 1850–1862. doi: 10.1007/s00376-025-4453-2.

View online: https://doi.org/10.1007/s00376-025-4453-2

ADVANCES IN ATMOSPHERIC SCIENCES, VOL. 42, SEPTEMBER 2025, 1850–1862

• **Original Paper** •

Weakening of Bomb Cyclones over the North Pacific in the Early 21st Century

Jiaxiang GAO[1,2], Rong-Hua ZHANG[*2], and Hai ZHI[3]

[1]*Jiangsu Key Laboratory of Atmospheric Environment Monitoring and Pollution Control*, *Collaborative Innovation Center of Atmospheric Environment and Equipment Technology*, *School of Environmental Science and Engineering*, *Nanjing University of Information Science and Technology*, *Nanjing* 210044, *China*

[2]*School of Marine Sciences*, *Nanjing University of Information Science and Technology*, *Nanjing* 210044, *China*

[3]*School of Atmospheric Sciences*, *Nanjing University of Information Science and Technology*, *Nanjing* 210044, *China*

(Received 29 October 2024; revised 3 January 2025; accepted 5 February 2025)

ABSTRACT

Bomb cyclones are rapidly deepening extratropical cyclones predominantly found in midlatitude regions. These extreme events are particularly frequent over the North Pacific (NP), posing significant societal and environmental risks. Currently, our understanding of the variability of bomb cyclones over the NP remains limited. This study analyzes the variations in multiple NP bomb cyclone characteristics from 1980 onward using four major reanalysis datasets. The results show a weakening trend of bomb cyclones since the beginning of the 21st century, which is characterized by significant reductions in maximum near-surface wind speeds, increases in minimum sea level pressure, and slower deepening rates. Further analysis reveals that the observed weakening trend of bomb cyclones is closely linked to a reduction in maximum 850 hPa Eady growth rate, driven primarily by reduced vertical wind shear within the 30°–45°N latitudinal band. Furthermore, our findings indicate that the Aleutian Low acts to modulate the meridional air temperature gradient over the midlatitude NP, which is corroborated by climate model outputs. This modulation provides a pathway for the Aleutian Low to affect low-level baroclinicity and thus bomb cyclone characteristics. These results have important implications for future projections of bomb cyclone activity over the NP, aiding in risk assessment and mitigating the impacts of these extreme events.

Key words: bomb cyclones, maximum near-surface wind, Eady growth rate, meridional air temperature gradient, North Pacific

Citation: Gao, J. X., R.-H. Zhang, and H. Zhi, 2025: Weakening of bomb cyclones over the North Pacific in the early 21st century. *Adv. Atmos. Sci.*, **42**(9), 1850−1862, https://doi.org/10.1007/s00376-025-4453-2.

Article Highlights:

- Bomb cyclones over the North Pacific weaken from 2001, featuring reduced maximum wind speeds and slower deepening rates.
- Annual variations in bomb cyclone characteristics are positively correlated with variations in the low-level Eady growth rate.
- Modulation of meridional air temperature gradients by the Aleutian Low affects the Eady growth rate and thus bomb cyclones.

1. Introduction

Bomb cyclones, also known as explosive cyclones, are intense extratropical storms characterized by a rapid decrease in their central pressure. Typically, a bomb cyclone is defined as an extratropical cyclone with a central pressure drop of at least 24 hPa within a 24-hour period (Sanders and Gyakum, 1980). This rapid intensification results in severe weather conditions, including high winds, heavy precipitation, and coastal flooding, making bomb cyclones highly significant in both meteorological and societal terms (Hewson and Neu, 2015; Fu et al., 2023). Bomb cyclones usually occur in midlatitudes during the cold season and have historically caused significant damage to life and property in regions such as East Asia, North America, and Europe (Liberato et al., 2011; Booth et al., 2015; Brâncuş et al., 2019; Fu et al., 2024). Therefore, understanding the characteristics of bomb cyclones and how they are evolving under current climate is crucial for mitigating their impacts

* Corresponding author: Rong-Hua ZHANG
Email: rzhang@nuist.edu.cn

on both the environment and human society.

The North Pacific (NP) is one of the most active regions of bomb cyclone activity in the Northern Hemisphere (Kuwano-Yoshida and Minobe, 2017; Fu et al., 2023). The climatology of NP bomb cyclones has been well documented in previous studies (e.g., Allen et al., 2010; Zhang et al., 2017). These storms generally originate from both the Asian continent and the Pacific Ocean (Yoshida and Asuma, 2004). Fu et al. (2020) demonstrated that NP bomb cyclones frequently occur to the east of Japan and travel across the Pacific Ocean in southwest–northeast directions, potentially impacting coastal regions in East Asia and North America. The annual frequency of these events is highest during boreal winter, decreases slightly in spring and autumn, and is nearly zero in summer (Fu et al., 2020). Based on the European Centre for Medium-Range Weather Forecasts (ECMWF) interim reanalysis (ERA-Interim) from 1979 to 2018, Jiang et al. (2022) conducted a statistical analysis of the maximum surface winds associated with NP bomb cyclones. They found that the maximum wind speeds, typically around 30 m s^{-1}, generally occur after an event reaches its peak deepening during its lifecycle.

In addition, NP bomb cyclones exhibit interannual to interdecadal variabilities, which is essential to understand. An early study by Graham and Diaz (2001) reported a significant increase in the frequency of extreme cyclones over the NP from 1948/49 to 1997/98 using sea level pressure (SLP) reanalysis. More recently, Iwao et al. (2012) indicated a notable rise in explosive cyclone frequency east of Japan from 1979/1980 to 2010/11 using the Japanese 25-year Reanalysis and Japan Meteorological Agency (JMA) Climate Data Assimilation System dataset (JRA-25/JCDAS; Onogi et al., 2007). Consistently, Kuwano-Yoshida et al. (2022) noted a rapid increase in bomb cyclone activity over the mid-winter NP from the late 1980s, using the Japanese 55-year reanalysis assimilating only conventional observations (JRA-55C, Kobayashi et al., 2014). In contrast, Tilinina et al. (2013) found that the number of deep cyclones over the NP increased from the late 1980s, peaked around 2000, and then decreased in the 21st century, resulting in an insignificant linear trend from 1979 to 2010 across the examined reanalysis datasets. It is worth noting that most previous studies focused on cyclone activity (i.e., the number of events) rather than major characteristics of these events, such as the maximum near-surface wind speeds or minimum SLP. Although Graham and Diaz (2001) noted an intensification of cyclone extreme surface winds, this early work cannot help inform the variability of bomb cyclones in the 21st century.

Moreover, there remains considerable uncertainty regarding the drivers of NP bomb cyclone variability, especially with respect to the relative influence of global warming versus natural variability (Zhang et al., 1998). Iwao et al. (2012) argued that the identified increase in NP bomb cyclones agrees with the enhancement of storm tracks under global warming (Inatsu and Kimoto, 2005). A more recent study by Karwat et al. (2022) also found increased storminess over the NP in response to global warming. In contrast, Kuwano-Yoshida et al. (2022) attributed the recent changes in NP bomb cyclone activity to interdecadal environmental variability in this region. Furthermore, climate model projections from the Coupled Model Intercomparison Project, phase 5 (Taylor et al., 2012) and phase 6 (Eyring et al., 2016), both indicate that NP bomb cyclone activity tends to shift poleward under global warming (Seiler and Zwiers, 2016; Gao et al., 2024). This poleward movement would result in reduced bomb cyclone activity east of Japan, which is not quite consistent with the increases reported by Kuwano-Yoshida et al. (2022) and Karwat et al. (2022). Consequently, it remains unclear whether global warming has caused detectable changes in NP bomb cyclone behavior in the 21st century, which calls for further investigation into the factors driving their variability.

In this study, we aim to systematically examine the variability of bomb cyclone characteristics over the NP and its drivers from 1980 onward. We track and identify bomb cyclones in several reanalysis datasets, then assess the trends in multiple bomb cyclone characteristics. Furthermore, using both reanalysis and climate model outputs, we hope to clarify the environmental factors affecting variations in NP bomb cyclones and contribute to broader debates on how climate change is affecting these events. The rest of this paper is organized as follows. Section 2 details the data and methods. The trends in bomb cyclone characteristics and related analyses of environmental factors are presented in section 3. In section 4, we describe our major conclusions and discuss further implications of our findings.

2. Data and methods

2.1. *Datasets*

In this study, we use four reanalysis datasets to examine the variability of bomb cyclones: the fifth major global reanalysis produced by ECMWF (ERA5; Hersbach et al., 2020); ERA-Interim (Dee et al., 2011); NASA's Modern-Era Retrospective Analysis for Research and Applications, version 2 (MERRA2; Gelaro et al., 2017); and the JRA-55 reanalysis (Kobayashi et al., 2015). These datasets are well recognized for their overall good data quality and broad application in atmospheric research. Table 1 presents the spatial and temporal resolutions, along with the temporal coverage, of the four datasets used in this study. In addition, ERA5 is adopted to investigate the environmental factors affecting bomb cyclone variability. ERA5 is widely regarded for its high temporal and spatial resolutions, as well as its incorporation of a vast amount of observational data from satellites, weather stations, and buoys. The high quality of ERA5 and its superior spatial resolution make it particularly suitable for mechanism analysis, as compared to other reanalysis datasets examined here.

To strengthen confidence in the reanalysis results, we also analyze four climate models participating in the High-res-

Table 1. Reanalysis datasets and climate models examined in this study.

Source	Name	Spatial resolution	Temporal resolution	Temporal coverage
Reanalysis	ERA5	0.25° × 0.25°	6-hourly, daily, monthly	1980–2017
	ERA-Interim	0.75° × 0.75°	6-hourly	1980–2015
	JRA-55	0.56° × 0.56°	6-hourly	1980–2013
	MERRA2	0.5° × 0.625°	6-hourly	1981–2014
Climate model	MPI-ESM1-2-HR	~0.93° (atmosphere) 0.4° (ocean)	6-hourly, monthly	1950–2014
	EC-Earth3P	~1° (atmosphere) 1° (ocean)	6-hourly, monthly	1950–2014
	CMCC-CM2-HR4	1° (atmosphere) 0.25° (ocean)	6-hourly, monthly	1950–2014
	HadGEM3-GC31-MM	0.83° × 0.56° (atmosphere) 0.25° (ocean)	6-hourly, monthly	1950–2014

olution Model Intercomparison Project (HighResMIP; Haarsma et al., 2016): MPI-ESM1-2-HR (Gutjahr et al., 2019), EC-Earth3P (Haarsma et al., 2020), CMCC-CM2-HR4 (Cherchi et al., 2019), and HadGEM3-GC31-MM (Roberts et al., 2019). HighResMIP is one of the endorsed projects of CMIP6. We use coupled historical simulations performed by these models, covering the period 1950 to 2014. The external forcings for these simulations generally follow the standard CMIP6 historical simulations (Eyring et al., 2016) with fixed land use. The spatial and temporal resolutions of the analyzed models are also presented in Table 1. Additional details on model configurations and experimental designs can be found in Gao et al. (2024) and references therein. For this study, we analyze one ensemble member from each model.

Moreover, we examine three key climate indices—the Pacific Decadal Oscillation (PDO) index (Mantua and Hare, 2002), the Tripole Index (TPI) for the Interdecadal Pacific Oscillation (IPO; Henley et al., 2015), and the North Pacific Index (NPI; Trenberth and Hurrell, 1994)—to explore the relation between bomb cyclones and large-scale climate variability in the NP (Zhang and Levitus, 1997; Zhang et al., 1999; Di Lorenzo et al., 2023). The PDO index is obtained from the JMA. It captures the dominant mode of decadal SST variability in the NP. The TPI (IPO) index measures the phase of the IPO, a long-term Pacific climate variability pattern that influences the frequency and intensity of weather systems over the Pacific basin. Here, we use the unfiltered version of the TPI (IPO) index calculated from NOAA's ERSST.v5 (Henley et al., 2015). The NPI is obtained from the Climate Data Guide, which reflects the strength of the Aleutian Low, a semi-permanent low-pressure system over the NP. In this study, we use monthly values of these indices from 1980 onward.

2.2. *Analysis methods*

We perform cyclone tracking for the reanalysis datasets and climate models using the TRACK algorithm (Hodges, 1999; Hodges et al., 2011). The tracking is conducted on 6-hourly 850 hPa relative vorticity (RV) fields with T42 resolution smoothing, a configuration that has been widely validated in previous studies (e.g., Sinclair et al., 2020; Priestley and Catto, 2022). The 6-hour interval balances computational efficiency with the temporal resolution necessary to capture cyclone evolution. The 850 hPa RV is a well-established parameter for identifying cyclone centers. The T42 smoothing ensures comparable tracking results across different spatial resolutions. The TRACK algorithm identifies cyclones based on local RV maxima exceeding a threshold value of 1×10^{-5} s^{-1}, which are then linked in time to create continuous cyclone tracks. The algorithm also calculates multiple cyclone properties at each time step, including the storm's maximum near-surface wind speed, minimum SLP, and the associated geographic locations, which are important for our further investigation into bomb cyclone characteristics. To exclude transient events, only extratropical cyclones with a lifetime longer than 2 days are retained for subsequent bomb cyclone identification.

Bomb cyclone events are identified from extratropical cyclone tracks by examining the 24-hour deepening rate (DPR) of the central pressure minimum at each time step (except for the first and last two time steps). The 24-hour DPR is calculated as follows:

$$\mathrm{DPR} = \frac{p_{t-12\mathrm{h}} - p_{t+12\mathrm{h}}}{24} \times \left| \frac{\sin 60^\circ}{\sin \frac{\varphi_{t-12\mathrm{h}} + \varphi_{t+12\mathrm{h}}}{2}} \right|, \qquad (1)$$

where t represents the analyzed time step, and p and φ represent the SLP value (units: hPa) and latitude (units: °) of the pressure minimum, respectively. Equation (1) calculates the 24-hour pressure drop of a cyclone's central pressure minimum normalized at 60° as in Sanders and Gyakum (1980). The unit of measurement for DPR is bergerons, with one bergeron equal to a pressure drop of 24 hPa in 24 hours. To avoid the inclusion of tropical cyclones, we discard time steps when φ is equatorward of 30°N. If a cyclone has a 24-hour DPR larger than one bergeron during its lifetime, the event is categorized as a bomb cyclone.

We then examine the major characteristics of bomb cyclones using four different metrics: maximum near-surface wind speeds, minimum SLP, maximum RV, and maximum 24-hour DPR (the fastest rate of deepening for an event). While the maximum RV is directly derived from the measure-

ment of the cyclone center RV, we would like to note that the maximum near-surface wind speeds and the minimum SLP are not directly measured at the cyclone center but identified within a 5° geodesic radius of the center by the tracking algorithm (Bengtsson et al., 2009; Hodges et al., 2011). This method ensures that the relevant metrics capture the most extreme values associated with each bomb cyclone. As a result, the magnitudes of these metrics are larger than those directly derived from the RV center. However, the 5° radius is sufficiently small to accurately represent the core characteristics of the tracked cyclones, minimizing any potential impacts of this approach on our results. We evaluate these metrics for each bomb cyclone and then take the annual average across all events over the NP.

To explore environmental factors affecting the variability of bomb cyclone characteristics, we specifically calculate the maximum Eady growth rate (EGR; Lindzen and Farrell, 1980) at 850 hPa. The maximum EGR is calculated using daily ERA5 data (derived from 6-hourly data) with the following equation:

$$\mathrm{EGR} = 0.31\,|f|\left|\frac{\partial u}{\partial z}\right| N^{-1}\,. \tag{2}$$

In Eq. (2), f is the Coriolis frequency; $\partial u/\partial z$ is the vertical shear of the zonal wind speed u, in which z represents the geopotential height; and N is the Brunt–Väisälä frequency, calculated as

$$N = \left(\frac{g}{\theta}\frac{\partial \theta}{\partial z}\right)^{\frac{1}{2}}\,. \tag{3}$$

Here, g and θ are the gravitational acceleration and the potential temperature, respectively. Both $\partial u/\partial z$ and $\partial\theta/\partial z$ are calculated between 925 and 700 hPa.

3. Results

3.1. *Recent changes in bomb cyclone characteristics*

Figure 1 presents the tracks of bomb cyclones from 2001 to 2017 based on the ERA5 reanalysis. A total of 1155 events are identified, with an average of around 68 events per year. These bomb cyclones generally originate in East Asia or the NP, with their maximum near-surface wind speeds observed over the ocean. Therefore, we focus our analysis of bomb cyclone characteristics on events occurring within (30°–60°N, 120°E–120°W) (indicated by the green dashed lines in Fig. 1).

The annual variations in bomb cyclone characteristics since the 1980s are shown in Fig. 2. It is worth noting that steady trends can be observed for the examined metrics, especially during the 21st century. Therefore, we further quantify the trends in these annual statistics for three different periods: the whole reanalysis periods, the period before 2000 (from 1980 to 1999, except for MERRA2, whose statistics are available from 1981) and after 2000 (from 2001 onward). The resultant trends for different periods are summarized in Table 2, and their statistical significance is examined using a t-test. For the maximum near-surface wind speeds, three of the four examined reanalysis datasets display a decreasing trend since 2001, with ERA-Interim being the exception. It is worth noting that ERA5 has relatively low wind speeds compared to other datasets, which is possibly due to high drag coefficients used in the numerical model under extreme conditions (Bidlot et al., 2020). For the minimum SLP and maximum DPR, results from ERA5, JRA-55 and MERRA2 again show consistent trends since the beginning of the 21st century (the trend in the maximum DPR for ERA5 is significant at a 90% confidence level). For the maxi-

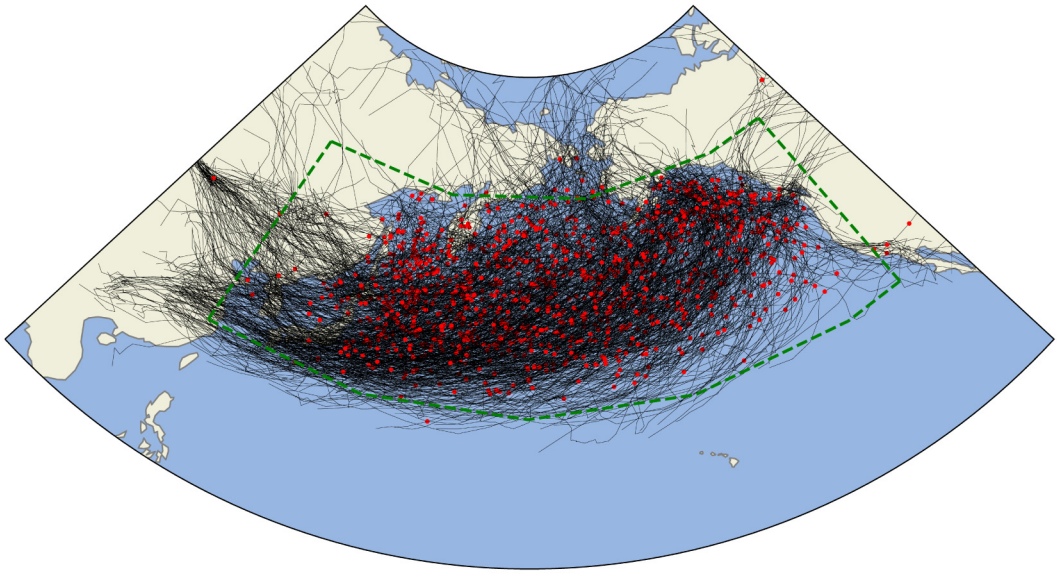

Fig. 1. Bomb cyclone tracks (black solid lines) over the NP in ERA5 during 2001–17. Red dots indicate the locations where the bomb cyclones exhibit maximum near-surface wind speeds. Green dashed lines indicate the region of (30°–60°N, 120°E–120°W).

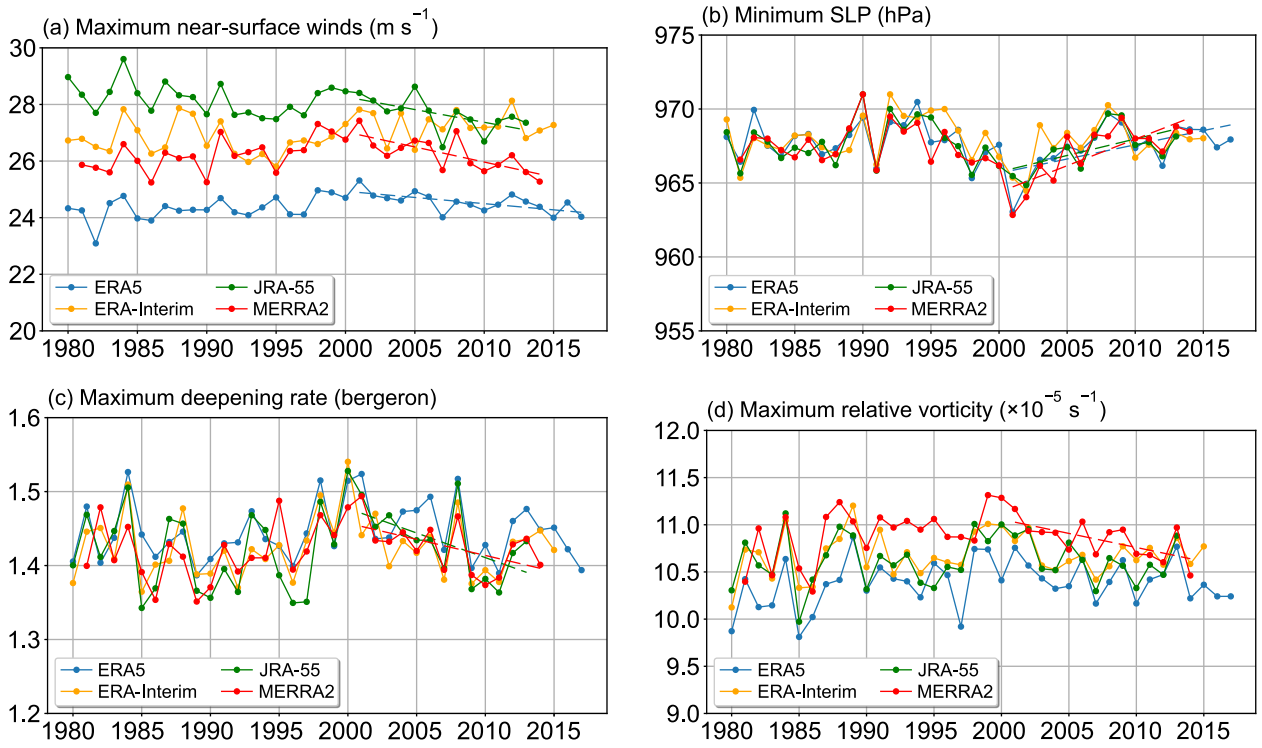

Fig. 2. Annual variations in bomb cyclone characteristics in four reanalysis datasets from 1980 onward. Regression lines are plotted for significant ($p < 0.05$) trends from 2001 onward.

Table 2. Trends in bomb cyclone and non-bomb cyclone characteristics during different time periods for four reanalysis datasets. Significant ($p < 0.05$) increasing and decreasing trends are shown in red and blue fonts, respectively.

Metric	Reanalysis	Bomb cyclone trends			Non-bomb cyclone trends		
		Whole period	Before 2000	After 2000	Whole period	Before 2000	After 2000
Maximum near-surface wind speed (m s^{-1} yr^{-1})	ERA5	0.009	0.028	−0.044	0.001	0.006	−0.012
	ERA-Interim	0.019	−0.022	−0.007	0.003	−0.003	0.007
	JRA-55	−0.036	−0.039	−0.090	−0.033	−0.024	−0.046
	MERRA2	0.004	0.054	−0.107	−0.007	−0.002	−0.035
Minimum sea-level pressure (hPa yr^{-1})	ERA5	−0.005	−0.008	0.192	0.036	0.032	0.046
	ERA-Interim	2×10^{-4}	0.082	0.115	0.028	0.004	0.050
	JRA-55	−0.006	0.031	0.223	0.029	−0.003	0.223
	MERRA2	−0.002	−0.003	0.358	0.033	−0.019	0.091
Maximum deepening rate (bergeron yr^{-1})	ERA5	2×10^{-4}	3×10^{-4}	−0.004	-2×10^{-4}	8×10^{-4}	-4×10^{-4}
	ERA-Interim	2×10^{-4}	6×10^{-4}	−0.001	-1×10^{-4}	0.001	-5×10^{-4}
	JRA-55	2×10^{-4}	−0.001	−0.007	-6×10^{-4}	5×10^{-4}	−0.002
	MERRA2	3×10^{-4}	0.001	−0.004	0	0.001	−0.001
Maximum relative vorticity (×10^{-5} s^{-1} yr^{-1})	ERA5	0.005	0.022	−0.014	−0.004	0.001	−0.016
	ERA-Interim	0.003	0.014	−0.001	−0.003	0.007	−0.016
	JRA-55	0.002	0.006	−0.018	−0.001	0.005	−0.021
	MERRA2	1×10^{-4}	0.024	−0.030	−0.005	0.010	−0.022

mum RV, all four datasets show a decreasing trend, though only the MERRA2 result is significant at a 95% confidence level. Overall, despite some differences between datasets and metrics, our results consistently suggest that bomb cyclones over the NP have weakened in the early 21st century.

In addition, we analyze the annual variations in the same metrics for non-bomb cyclones over the NP in Fig. 3 and Table 2. For the maximum near-surface wind speeds, a significant decreasing trend since 2001 is observed in the JRA-55 and MERRA2 results, but the magnitudes of these trends are smaller than those for bomb cyclones. Regarding the minimum SLP, only JRA-55 shows a significant increasing trend. The trends in the maximum DPR for non-bomb

cyclones after 2000 are insignificant across all examined datasets. In contrast, all four datasets display a significant decreasing trend in the maximum RV of non-bomb cyclones, indicating the RV trends are more pronounced for non-bomb cyclones than for bomb cyclones. This is probably because the cyclones are tracked based on RV, while bomb cyclones are identified by the DPR of SLP. Except for the maximum RV, the trends are generally larger in magnitude and more significant for bomb cyclones compared to non-bomb cyclones. These results suggest that NP bomb cyclones undergo more substantial changes than non-bomb cyclones in recent years, which highlights the importance of focusing on these extreme extratropical storms.

Given the observed weakening trend in bomb cyclones in the 21st century, we further compare the epoch-mean of bomb cyclone characteristics before and after 2000 in Fig. 4. The epoch-mean values are computed by directly averaging the relevant metrics of all bomb cyclone events occurring within the respective time periods. For the maximum near-surface wind speeds, while JRA-55 indicates that the events after 2000 are generally weaker than those before 2000, ERA-Interim shows an opposite result, indicating an increase in the wind speeds after 2000. The epoch differences for ERA5 and MERRA2 in Fig. 4a are insignificant, despite the significant decreasing trends seen in Fig. 2a. For the minimum SLP, maximum RV and maximum DPR, the epoch differences are also insignificant across all datasets. Similarly, for non-bomb cyclones, systematic differences cannot be identified between the epoch-means before and after 2000 [see Fig. S1 in the electronic supplementary material (ESM)]. While the weakening of bomb cyclones in the 21st century does not necessarily lead to significant epoch differences before and after 2000, the lack of notable differences suggests that the observed trends are unlikely to have been induced by a monotonic forcing dating back to the 1980s. Given the steady rise in global mean temperature since the 1950s (IPCC, 2021), the absence of a steady trend in bomb cyclone characteristics for the whole analysis period (Table 2 and Fig. 4) implies that the recent weakening trends are more likely a result of natural climate variability, rather than anthropogenic influences. In the following sections, we seek to further investigate this hypothesis by analyzing environmental factors related to the observed trends.

3.2. *Analyses of local environmental factors*

To investigate the underlying mechanisms behind the variability of bomb cyclones, we conduct a correlation analysis between bomb cyclone characteristics and environmental variables over the NP using ERA5 (note that the pressure-level data used in the following analysis are not affected by the bias caused by drag coefficients). Previously, Seiler and Zwiers (2016) and Gao et al. (2024) both noted that bomb cyclone changes are closely associated with low-level EGR. Therefore, we first correlate the annual variations in NP bomb cyclone characteristics (as shown in Fig. 2) with the annual mean maximum 850 hPa EGR (derived from daily values) at each grid point during the same period (1980–2017). The correlation map for the maximum near-surface wind speeds is shown in Fig. 5a, while the results for other metrics can be found in Figs. S2a, S3a, and S4a in the ESM. Signifi-

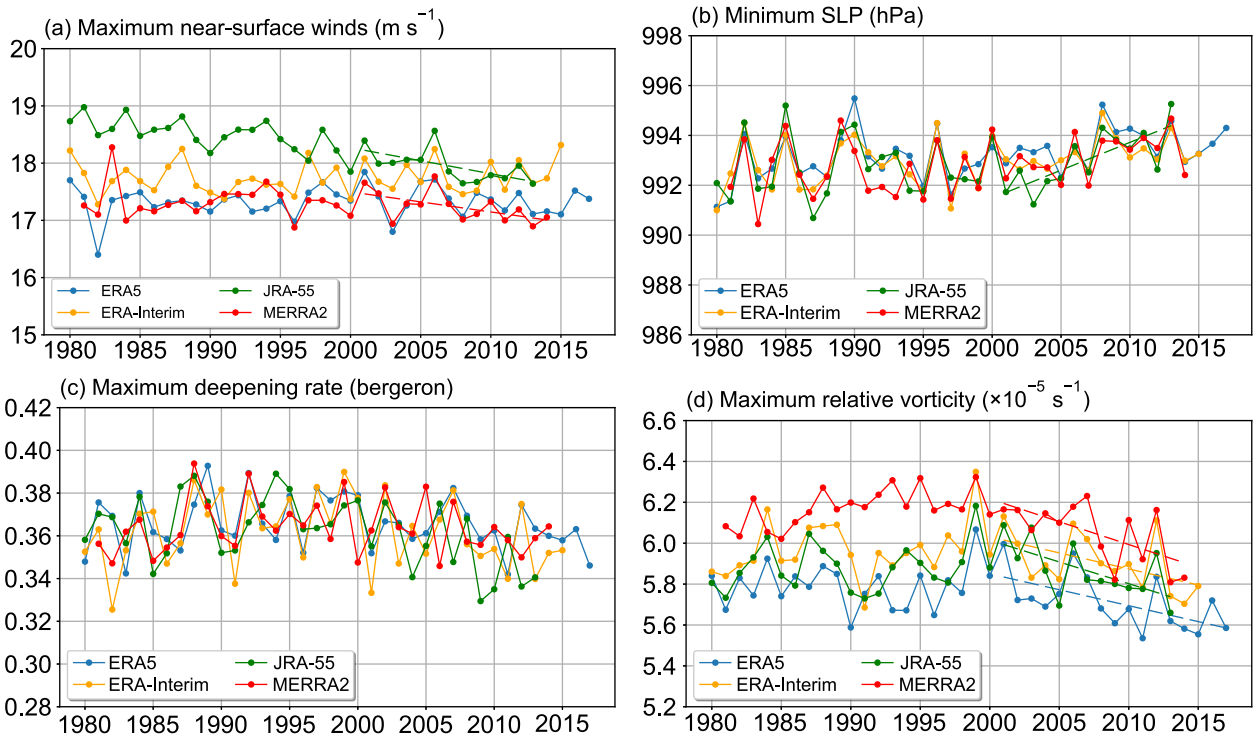

Fig. 3. Same as Fig. 2 but for non-bomb cyclones.

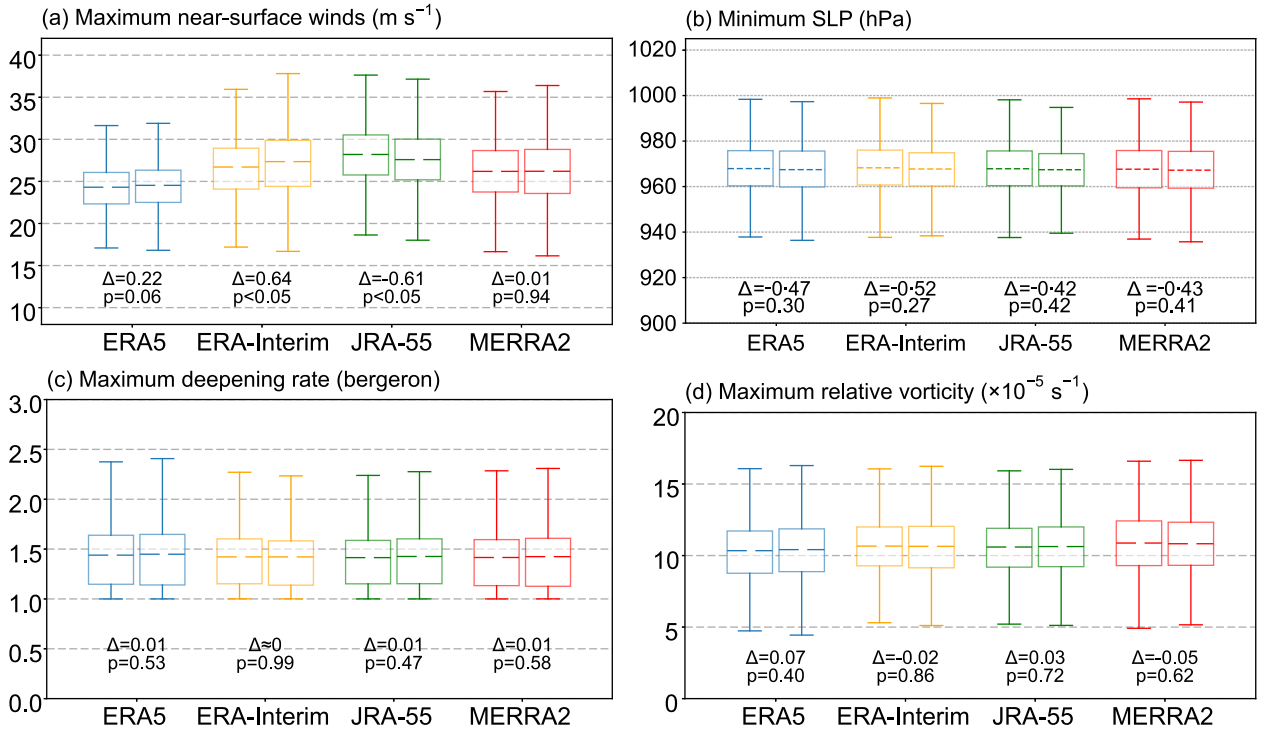

Fig. 4. Box plots for epoch mean bomb cyclone characteristic. In each panel, for the same dataset, the left-hand (right-hand) box is derived from the relevant metrics of all bomb cyclone events occurring before (after) the year 2000. The dashed lines represent the mean values for respective time periods.

cant positive correlations are observed in the 30°–45°N latitudinal band of the NP (Fig. 5a), with significant negative correlations generally outside the midlatitude NP. Similar correlation patterns with the maximum EGR are evident for other metrics as well (Figs. S2a, S3a, and S4a in the ESM). Given that the influence of low-level baroclinity on bomb cyclones is primarily localized, the significant correlations outside the midlatitude NP are likely caused by co-variability of large-scale EGR patterns rather than direct dynamical interactions. It is thus suggested that the annual variations in low-level baroclinity within 30°–45°N of the NP plays a dominant role in the observed weakening of bomb cyclones.

The maximum EGR is influenced by two terms as shown in Eq. (1): the static stability (i.e., the Brunt–Väisälä frequency) and the vertical zonal wind shear. To further investigate the contribution of each term to bomb cyclone variability, we calculate the correlation maps between the annual variations in these terms and the maximum near-surface wind speeds (for other metrics, see Figs. S2–S4 in the ESM), as shown in Figs. 5b and c. The spatial correlation pattern for the vertical zonal wind shear (Fig. 5b) is similar to that of the maximum EGR, featuring significant positive correlations within the 30°–45°N latitudinal band. In contrast, the correlation results for static stability are generally negative over the whole NP, with significant correlations largely found outside the analysis region (Fig. 5c). Consequently, the consistent positive correlations observed in Figs. 5a and b highlight the dominant role of vertical zonal wind shear in driving the association between bomb cyclone variability and maximum EGR.

As the vertical zonal wind shear is closely linked to the spatial distribution of low-level temperature through the thermal wind relationship, we incorporate the meridional air temperature gradient at 1000 hPa into our correlation analysis. The correlation maps for the maximum near-surface wind speeds are presented in Fig. 5d (for other metrics, see Figs. S2–S4 in the ESM). Notably, the correlation results closely resemble those in Figs. 5a and b, with significant positive correlations concentrated within the 30°–45°N latitudinal band, albeit with slightly noisier patterns. This similarity underscores the role of the low-level meridional temperature gradient in modulating the vertical wind shear and subsequently the maximum EGR. Therefore, the observed weakening of bomb cyclones can be attributed to the changes in the low-level meridional temperature gradient over the NP. To further validate this association, we calculate the annual mean meridional air temperature gradient at 1000 hPa averaged over (30°–45°N, 120°E–120°W) and correlate it with the annual mean maximum near-surface wind speeds of bomb cyclones from 1980 to 2017 in Fig. 6. The significant correlation in Fig. 6 confirms the important role of the meridional temperature gradient in driving interannual variations in NP bomb cyclone characteristics.

3.3. *Linkage with large-scale variability*

Given the close relation between the bomb cyclone characteristics and meridional air temperature gradient, it is desirable to further explore whether this relationship can be under-

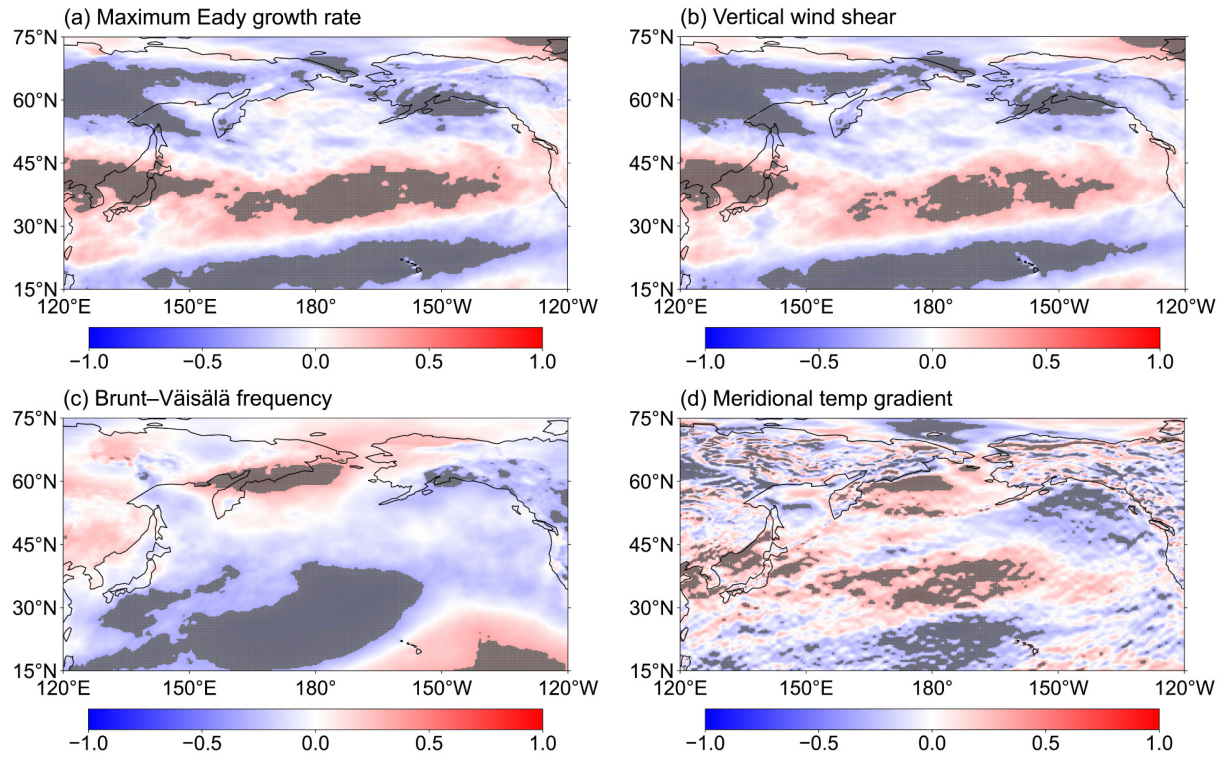

Fig. 5. Correlation maps between the annual variations in the maximum near-surface wind speeds of bomb cyclones over the NP and four environmental variables from 1980 to 2017. Shading indicates significant correlations with $p < 0.05$.

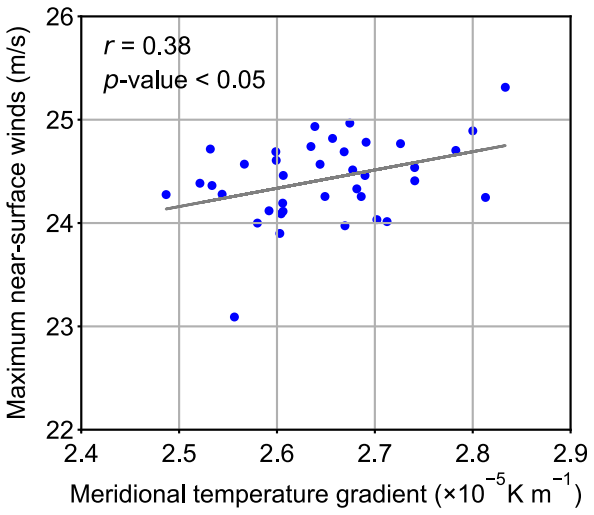

Fig. 6. Scatter plot between the annual variations in the maximum near-surface wind speeds of bomb cyclones over the NP and the 1000 hPa meridional air temperature gradient averaged over (30°–45°N, 120°E–120°W) from 1980 to 2017.

stood in the context of large-scale climate variability in the NP. Therefore, we calculate the annual averages of the PDO, IPO, and NPI indices using their monthly values. We then perform a min–max normalization on the annual climate indices, the annual mean maximum near-surface wind speeds, and meridional air temperature gradient (the two variables shown in Fig. 6). The normalized results for 2001–17 are shown in Fig. 7a to provide a quick examination of the variations in these variables during the 21st century. It is indicated that the normalized maximum near-surface wind speeds and temperature gradient correspond well throughout the analysis period, which agrees with our above analysis. Although all three climate indices exhibit negative correlations with the maximum wind speeds, we note the NPI shows relatively good correspondence with the temperature gradient. To further explore their relationship, monthly NPI values are plotted against the monthly 1000 hPa meridional air temperature gradient averaged over (30°–45°N, 120°E–120°W) from 1980 to 2017 in Fig. 7b. A significant negative correlation is observed between the two variables, confirming their linkage. It is worth noting that, while the linear regression yields a p-value < 0.05, the relationship in Fig. 7b appears to be nonlinear. This suggests that the interaction between the NPI and the low-level temperature gradient cannot be fully captured by linear regression, but a further investigation is beyond the scope of the current analysis. Similar correlation analysis using monthly values for the PDO and IPO indices are also conducted, and the results are insignificant (not shown).

Consequently, Fig. 7 suggests the NPI plays an important role in modulating the meridional air temperature gradient over the lower midlatitudes of the NP. Specifically, a high (low) NPI corresponds to a weakened (enhanced) low-level meridional air temperature gradient in this region. Changes in the meridional temperature gradient in turn affect the local vertical zonal wind shear through the thermal wind relationship, thereby modulating the low-level baroclinity.

These processes provide a dynamic pathway through which large-scale atmospheric variability in the NP, as represented by the NPI, impacts bomb cyclones in this region. Moreover, these results suggest that the variability of large-scale atmospheric circulation, rather than large-scale SST patterns, is primarily responsible for the recent weakening of bomb cyclones over the NP.

3.4. *Climate model results*

While we have identified a close association among the annual variations in NP bomb cyclone characteristics, the meridional air temperature gradient, and the NPI, it is desirable to further validate these relationships with climate model outputs given the relatively short temporal coverage of the ERA5 data. We thus calculate the annual variations in bomb cyclone characteristics, as well as the meridional air temperature gradient at 1000 hPa [averaged over (30°–45°N, 120°E–120°W)] and the NPI, for the period 1950–2014, for the four HighResMIP models in Table 1. The annual NPI and temperature gradient for the models are derived from monthly mean model outputs. Correlations between these variables are presented in Table 3, with the maximum near-surface wind speeds of bomb cyclones serving as the representative metric for the examined bomb cyclone characteristics, as in section 3.3.

Table 3 shows that all examined models successfully reproduce the observed close association between the NPI and the temperature gradient in the lower midlatitude NP. Notably, for the CMCC-CM2-HR4 model, this correlation becomes significant only when the NPI leads the temperature gradient by one year, suggesting a lagged impact of the NPI on the NP environment in this specific model. Despite this hysteresis, the models effectively capture the co-variability between the Aleutian Low and the low-level temperature gradient over the NP. Actually, the scatter plots between these two variables using monthly mean values for the models are nearly identical to Fig. 7b (not shown), indicating that the nonlinear correlation observed in reanalysis data is also well captured by coupled simulations.

However, only one model (MPI-ESM1-2-HR) among the four examined shows a significant correlation between the maximum near-surface wind speeds of bomb cyclones and the meridional temperature gradient. It is worth noting that the MPI-ESM1-2-HR model also exhibits a close connection between the NPI and the maximum wind speeds. This means that the dynamical pathway discussed in section 3.3 is well simulated in this model. In contrast, the other three models generally have difficulty in reproducing the influence of the low-level temperature gradient on NP bomb cyclones. This discrepancy may stem from differences in model

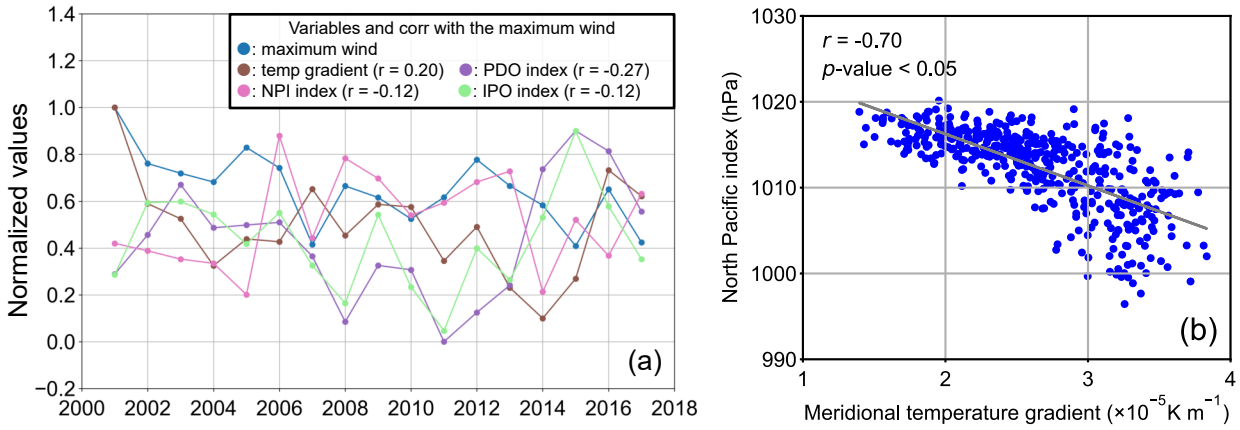

Fig. 7. (a) Time series of the min–max normalized annual variations in the maximum near-surface wind speeds of bomb cyclones over the North Pacific (blue), the 1000 hPa meridional air temperature gradient averaged over (30°–45°N, 120°E–120°W) (brown), the PDO index (purple), the NPI (pink), and the IPO index (green), from 2001 to 2017. (b) Scatter plot between the monthly North Pacific Index and 1000 hPa meridional air temperature gradient averaged over (30°–45°N, 120°E–120°W) from 1980 to 2017, with the linear regression result.

Table 3. Correlation coefficients between the annual mean variations in the maximum near-surface wind speeds of bomb cyclones and environmental factors during 1950 to 2014 for the HighResMIP models. Bold font indicates that the correlation is significant at $p < 0.05$. An asterisk (*) indicates the correlation result when the NPI leads by one year).

	Correlation coefficients between annual mean variables		
HighResMIP model	NPI & meridional temp gradient	NPI & maximum wind	Meridional temp gradient & maximum wind
MPI-ESM1-2-HR	**−0.37**	**−0.31**	**0.25**
EC-Earth3P	**−0.26**	−0.20	0.11
CMCC-CM2-HR4	−0.21 (**−0.40***)	−0.23	0.16
HadGEM3-GC31-MM	**−0.27**	−0.04	0.16

physics and parameterizations, which significantly impact how extreme weather events are represented in coupled climate models. Moreover, it is possible that interannual variability in bomb cyclone characteristics within these models is driven by other factors, such as upper-level jet streams, though a more in-depth analysis of the underlying mechanisms is not the objective of this study.

4. Discussion and conclusions

In this study, we have systematically examined the variations in NP bomb cyclone characteristics from 1980 onward using four reanalysis datasets. Our results reveal a clear weakening trend in NP bomb cyclones since the beginning of the 21st century. Specifically, we find consistent reductions in the maximum near-surface wind speeds, increases in the minimum SLP, and declines in the maximum DPR for NP bomb cyclones. These trends are particularly evident in ERA5, JRA-55, and MERRA2, whereas ERA-Interim shows some inconsistencies. In addition, we contrast the variability of these metrics between bomb cyclones and non-bomb cyclones. Although non-bomb cyclones show a clear weakening trend in their maximum RV, the trends in wind, SLP and DPR are less pronounced than those for bomb cyclones. Overall, our findings highlight that NP bomb cyclones are becoming less intense as measured by multiple metrics, marking a significant shift in their behavior in the early 21st century.

In our analysis, ERA-Interim usually stands out as the only dataset that is inconsistent with the others. Notably, ERA-Interim has the coarsest horizontal resolution among the examined reanalysis datasets. Previously, Gao et al. (2020) highlighted the sensitivity of bomb cyclone characteristics to horizontal resolution, indicating that the frequency of small-scale events and their associated wind speeds might be inadequately represented in lower-resolution datasets like ERA-Interim. This limitation likely contributes to the insignificant trends (Fig. 2) and distinct epoch-mean values (Fig. 4a) observed in ERA-Interim. In addition, differences in data assimilation methodologies and model physics may further contribute to the discrepancies found in ERA-Interim results. However, a detailed investigation of these factors is beyond the scope of this study. Despite these issues, the general agreement across the other datasets with varying resolutions suggests that factors such as spatial resolution do not significantly undermine the validity of our main conclusion regarding the weakening trend of bomb cyclones.

We have also investigated the underlying mechanisms behind the observed weakening of bomb cyclones. Our analysis focuses on the relationship between bomb cyclone characteristics and low-level baroclinity, assessed using the 850 hPa maximum EGR. The results indicate that the weakening of bomb cyclones is closely associated with a reduction in the maximum EGR within the 30°N–45°N latitudinal band, which is mainly caused by the influence of the meridional air temperature gradient on vertical zonal wind shear. Consistent with the localized influence of low-level baroclinity on cyclone development, our analysis of bomb cyclone characteristics within the 30°–45°N and 45°–60°N bands (Figs. S5 and S6 in the ESM) reveals that the weakening trend is actually predominantly attributable to lower-latitude events.

Furthermore, we seek to explain the variability of bomb cyclone characteristics in the context of large-scale climate variability. It is demonstrated that the NPI, which reflects the strength of the Aleutian Low, is a key factor behind the recent weakening of bomb cyclones. In Fig. 8, we provide a schematic showing how the Aleutian Low influences bomb cyclones over the NP. Specifically, the variability of the Aleutian Low causes temperature anomalies over the NP by altering wind patterns and heat fluxes (Wang et al., 2012; Di Lorenzo et al., 2023). As shown in Fig. 8, when the NPI exceeds its 90th percentile during 1980–2017, the western and central NP exhibits positive temperature anomalies,

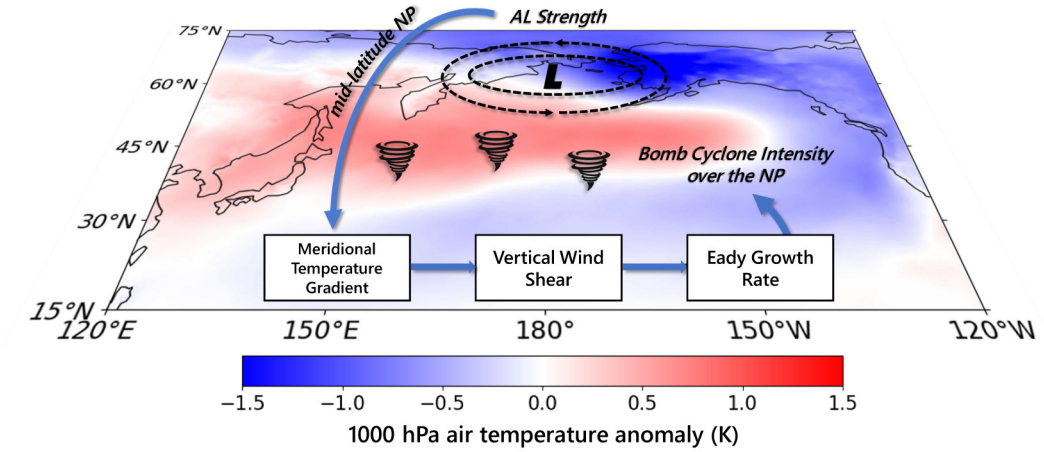

Fig. 8. A schematic illustrating the processes by which the Aleutian Low influences bomb cyclone characteristics. Colors represent the 1000 hPa air temperature anomalies averaged over months when the NPI exceeds its 90th percentile during 1980–2017.

with negative anomalies in other areas. This spatial pattern indicates a reduction in the temperature differences between the northern and southern NP, thereby weakening the low-level meridional air temperature gradient in the midlatitudes. Consistently, Zheng et al. (2024) pointed out that the variations in the strength of the spring Aleutian Low lead to meridional SST gradient anomalies in the midlatitude NP. Moreover, our model validation results confirm the connection between the NPI and large-scale NP environment, supporting our explanation of how the NPI modulates bomb cyclone characteristics. Notably, one model successfully reproduces the impact of the low-level temperature gradient on bomb cyclone characteristics, which helps to validate the dynamical pathway identified in the reanalysis results. However, large uncertainty remains in the representation of bomb cyclone behavior in coupled simulations, highlighting the necessity for further investigation.

The central role of the NPI suggests that the recent changes in bomb cyclone characteristics over the NP are primarily driven by natural atmospheric variability instead of anthropogenic influences. This result has important implications for the projection and attribution of future bomb cyclone changes. A key question on this topic is the extent to which the projected changes in bomb cyclones are influenced by natural variability versus the long-term impacts of global warming. Our analysis provides a better understanding of the connection between NP bomb cyclone behavior and natural variability, allowing for more confident attribution of future changes in cyclone behavior to intrinsic climate fluctuations and external drivers such as global warming.

There are, however, several caveats to this analysis. While we use multiple reanalysis datasets to ensure robustness, uncertainty remains regarding the observed weakening of bomb cyclones. Specifically, the fact that we only use a single cyclone tracking algorithm (based on RV) limits the potential for comparing our results with those derived from other tracking methods. For example, Graham and Diaz (2001) found a steady intensification trend in extreme cyclones from 1948/49 to 1997/98 in the central NP by tracking SLP reanalysis data, while our analysis of the period 1980–2000 fails to identify any significant trends across the four reanalysis datasets. Even within our analysis, we note that the trends in the maximum RV are much more pronounced for non-bomb cyclones than bomb cyclones, further suggesting that trends in certain metrics are sensitive to the specific cyclone filtering criteria used. Furthermore, the relatively short period covered by the reanalysis datasets (mostly since 1980) also constrains our ability to capture long-term trends in bomb cyclone behavior dating back to the pre-industrial era. As a result, we cannot fully rule out the possibility that global warming has already caused detectable changes in bomb cyclone characteristics. Future research should aim to further explore the interplays among natural climate variability, anthropogenic influences, and bomb cyclone activity by incorporating new observational datasets, additional cyclone tracking algorithms, and climate model simulations.

Acknowledgements. This research was supported by the National Natural Science Foundation of China (Grant No. 42030410), the Laoshan Laboratory (Grant Nos. LSKJ202202404 and LSKJ202202403), the Startup Foundation for Introducing Talent of NUIST, Jiangsu Innovation Research Group (Grant No. JSSCTD202346), and the Jiangsu Funding Program for Excellent Postdoctoral Talent (Grant No. 2023ZB690).

Electronic supplementary material: Supplementary material is available in the online version of this article at https://doi.org/10.1007/s00376-025-4453-2.

Data availability. The reanalysis and model data that support the findings of this study are openly available and can be accessed at the following links: https://doi.org/10.5065/D6CR5RD9 (ERA-Interim); https://doi.org/10.24381/cds.adbb2d47 (ERA5); https://doi.org/10.5065/D6HH6H41 (JRA55); and https://doi.org/10.5067/A7S6XP56VZWS (MERRA2). The HighResMIP simulation output can be obtained via the Earth System Grid Federation nodes, e.g., https://esgf-node.llnl.gov/projects/cmip6/. The extratropical cyclone tracking data are available from the corresponding author upon reasonable request.

REFERENCES

Allen, J. T., A. B. Pezza, and M. T. Black, 2010: Explosive cyclogenesis: A global climatology comparing multiple reanalyses. *J. Climate*, **23**, 6 468–6 484, https://doi.org/10.1175/2010JCLI3437.1.

Bengtsson, L., K. I. Hodges, and N. Keenlyside, 2009: Will extratropical storms intensify in a warmer climate? *J. Climate*, **22**(9), 2 276–2 301, https://doi.org/10.1175/2008JCLI2678.1.

Bidlot, J. R., F. Prates, R. Ribas, A. Mueller-Quintino, M. Crepulja, and F. Vitart, 2020: Enhancing tropical cyclone wind forecasts. ECMWF Newsletter, Number 164. Available from https://www.ecmwf.int/en/newsletter/164/meteorology/enhancing-tropical-cyclone-wind-forecasts.

Booth, J. F., H. E. Rieder, D. E. Lee, and Y. Kushnir, 2015: The paths of extratropical cyclones associated with wintertime high-wind events in the northeastern United States. *J. Appl. Meteorol. Climatol.*, **54**(9), 1 871–1 885, https://doi.org/10.1175/JAMC-D-14-0320.1.

Brâncuş, M., D. M. Schultz, B. Antonescu, C. Dearden, and S. Ştefan, 2019: Origin of strong winds in an explosive Mediterranean extratropical cyclone. *Mon. Wea. Rev.*, **147**(10), 3 649–3 671, https://doi.org/10.1175/MWR-D-19-0009.1.

Cherchi, A., and Coauthors, 2019: Global mean climate and main patterns of variability in the CMCC-CM2 coupled model. *Journal of Advances in Modeling Earth Systems*, **11**(1), 185–209, https://doi.org/10.1029/2018MS001369.

Dee, D. P., and Coauthors, 2011: The ERA-Interim reanalysis: Configuration and performance of the data assimilation system. *Quart. J. Roy. Meteor. Soc.*, **137**(656), 553–597, https://doi.org/10.1002/qj.828.

Di Lorenzo, E., and Coauthors, 2023: Modes and mechanisms of Pacific decadal-scale variability. *Annual Review of Marine Science*, **15**(1), 249–275, https://doi.org/10.1146/annurev-marine-040422-084555.

Eyring, V., S. Bony, G. A. Meehl, C. A. Senior, B. Stevens, R. J.

Stouffer, and K. E. Taylor, 2016: Overview of the Coupled Model Intercomparison Project Phase 6 (CMIP6) experimental design and organization. *Geoscientific Model Development*, **9**(5), 1 937–1 958, https://doi.org/10.5194/gmd-9-1937-2016.

Fu, G., Y. W. Sun, J. L. Sun, and P. Y. Li, 2020: A 38-year climatology of explosive cyclones over the Northern Hemisphere. *Adv. Atmos. Sci.*, **37**, 143–159, https://doi.org/10.1007/s00376-019-9106-x.

Fu, G., P. Y. Li, L. J. Chen, Y. M. Peng, and J. Ni, 2023: Historic and future perspectives of storm and cyclone. *Adv. Atmos. Sci.*, **40**, 447–463, https://doi.org/10.1007/s00376-022-2184-1.

Fu, S. M., H. Ma, and L. Z. Jiang, 2024: Increasing risks of the explosive extratropical cyclones over the North Atlantic storm track: A perspective from their surface wind maxima. *Environmental Research Letters*, **19**(5), 054 009, https://doi.org/10.1088/1748-9326/ad3b24.

Gao, J. X., and Coauthors, 2020: Influence of model resolution on bomb cyclones revealed by HighResMIP-PRIMAVERA simulations. *Environmental Research Letters*, **15**(8), 084001, https://doi.org/10.1088/1748-9326/ab88fa.

Gao, J. X., S. Minobe, M. J. Roberts, R. Haarsma, D. Putrasahan, E. Scoccimarro, L. Terray, and P. L. Vidale, 2024: Projected future changes in bomb cyclones by the HighResMIP-PRIMAVERA multimodel ensemble. *Climate Dyn.*, **62**, 8 121–8 135, https://doi.org/10.1007/s00382-024-07327-7.

Gelaro, R., and Coauthors, 2017: The modern-era retrospective analysis for research and applications, version 2 (MERRA-2). *J. Climate*, **30**(14), 5 419–5 454, https://doi.org/10.1175/JCLI-D-16-0758.1.

Graham, N. E., and H. F. Diaz, 2001: Evidence for intensification of North Pacific winter cyclones since 1948. *Bull. Amer. Meteor. Soc.*, **82**, 1 869–1 894, https://doi.org/10.1175/1520-0477(2001)082<1869:EFIONP>2.3.CO;2.

Gutjahr, O., D. Putrasahan, K. Lohmann, J. H. Jungclaus, J. S. Von Storch, N. Brüggemann, H. Haak, and A. Stössel, 2019: Max planck institute earth system model (MPI-ESM1.2) for the high-resolution model intercomparison project (HighResMIP). *Geoscientific Model Development*, **12**(7), 3 241–3 281, https://doi.org/10.5194/gmd-12-3241-2019.

Haarsma, R. J., and Coauthors, 2016: High resolution model intercomparison project (HighResMIP v1.0) for CMIP6. *Geoscientific Model Development*, **9**(11), 4 185–4 208, https://doi.org/10.5194/gmd-9-4185-2016.

Haarsma, R. J., and Coauthors, 2020: HighResMIP versions of EC-Earth: EC-Earth3P and EC-Earth3P-HR–description, model computational performance and basic validation. *Geoscientific Model Development*, **13**(8), 3 507–3 527, https://doi.org/10.5194/gmd-13-3507-2020.

Henley, B.J., J. Gergis, D. J. Karoly, S. Power, J. Kennedy, and C. K. Folland, 2015: A tripole index for the interdecadal pacific oscillation. *Climate Dyn.*, **45**(11–12), 3 077–3 090, https://doi.org/10.1007/s00382-015-2525-1.

Hersbach, H., and Coauthors, 2020: The ERA5 global reanalysis. *Quart. J. Roy. Meteor. Soc.*, **146**(730), 1 999–2 049, https://doi.org/10.1002/qj.3803.

Hewson, T. D., and U. Neu, 2015: Cyclones, windstorms and the IMILAST project. *Tellus A: Dynamic Meteorology and Oceanography*, **67**(1), 27 128, https://doi.org/10.3402/tellusa.v67.27128.

Hodges, K. I., 1999: Adaptive constraints for feature tracking. *Mon. Wea. Rev.*, **127**(6), 1 362–1 373, https://doi.org/10.1175/1520-0493(1999)127<1362:ACFFT>2.0.CO;2.

Hodges, K. I., R.W. Lee, and L. Bengtsson, 2011: A comparison of extratropical cyclones in recent reanalyses ERA-Interim, NASA MERRA, NCEP CFSR, and JRA-25. *J. Climate*, **24**(18), 4 888–4 906, https://doi.org/10.1175/2011JCLI4097.1.

Inatsu, M., and M. Kimoto, 2005: Two types of interannual variability of the mid-winter storm-tracks and their relationship to global warming. *SOLA*, **1**, 61–64, https://doi.org/10.2151/sola.2005-017.

IPCC, 2021: Summary for policymakers. *Climate Change 2021-The Physical Science Basis. Contribution of Working Group I to the Sixth Assessment Report of the Intergovernmental Panel on Climate Change*, Cambridge University Press, Cambridge, United Kingdom and New York, NY, USA, 3–32, https://doi.org/10.1017/9781009157896.001.

Iwao, K., M. Inatsu, and M. Kimoto, 2012: Recent changes in explosively developing extratropical cyclones over the winter northwestern Pacific. *J. Climate*, **25**, 7 282–7 296, https://doi.org/10.1175/JCLI-D-11-00373.1.

Jiang, L. Z., S. M. Fu, J. H. Sun, R. Fu, W. L. Li, S. X. Zhao, and H. Wang, 2022: Surface wind and vertical extent features of the explosive cyclones in the Northern Hemisphere based on the ERA-I reanalysis data. *International Journal of Climatology*, **42**(2), 993–1 014, https://doi.org/10.1002/joc.7284.

Karwat, A., C. L. E. Franzke, and R. Blender, 2022: Long-term trends of Northern Hemispheric winter cyclones in the extended ERA5 reanalysis. *J. Geophys. Res.: Atmos.*, **127**(22), e2022JD036 952, https://doi.org/10.1029/2022JD036952.

Kobayashi, C., H. Endo, Y. Ota, S. Kobayashi, H. Onoda, Y. Harada, K. Onogi, and H. Kamahori, 2014: Preliminary results of the JRA-55C, an atmospheric reanalysis assimilating conventional observations only. *SOLA*, **10**, 78–82, https://doi.org/10.2151/sola.2014-016.

Kobayashi, S., and Coauthors, 2015: The JRA-55 reanalysis: General specifications and basic characteristics. *J. Meteor. Soc. Japan*, **93**(1), 5–48, https://doi.org/10.2151/jmsj.2015-001.

Kuwano-Yoshida, A., and S. Minobe, 2017: Storm-track response to SST fronts in the Northwestern Pacific Region in an AGCM. *J. Climate*, **30**(3), 1 081–1 102, https://doi.org/10.1175/JCLI-D-16-0331.1.

Kuwano-Yoshida, A., S. Okajima, and H. Nakamura, 2022: Rapid increase of explosive cyclone activity over the midwinter North Pacific in the late 1980s. *J. Climate*, **35**(3), 1 113–1 133, https://doi.org/10.1175/JCLI-D-21-0287.1.

Liberato, M. L. R., J. G. Pinto, I. F. Trigo, and R. M. Trigo, 2011: Klaus–an exceptional winter storm over northern Iberia and southern France. *Weather*, **66**(12), 330–334, https://doi.org/10.1002/wea.755.

Lindzen, R. S., and B. Farrell, 1980: A simple approximate result for the maximum growth rate of baroclinic instabilities. *J. Atmos. Sci.*, **37**(7), 1 648–1 654, https://doi.org/10.1175/1520-0469(1980)037<1648:ASARFT>2.0.CO;2.

Mantua, N. J., and S. R. Hare, 2002: The Pacific decadal oscillation. *Journal of Oceanography*, **58**, 35–44, https://doi.org/10.1023/A:1015820616384.

Onogi, K., and Coauthors, 2007: The JRA-25 reanalysis. *J. Meteor. Soc. Japan*, **85**(3), 369–432, https://doi.org/10.2151/jmsj.85.369.

Priestley, M. D. K., and J. L. Catto, 2022: Future changes in the

extratropical storm tracks and cyclone intensity, wind speed, and structure. *Weather and Climate Dynamics*, **3**, 337–360, https://doi.org/10.5194/wcd-3-337-2022.

Roberts, M. J., and Coauthors, 2019: Description of the resolution hierarchy of the global coupled HadGEM3-GC3.1 model as used in CMIP6 HighResMIP experiments. *Geoscientific Model Development*, **12**(12), 4 999–5 028, https://doi.org/10.5194/gmd-12-4999-2019.

Sanders, F., and J. R. Gyakum, 1980: Synoptic-dynamic climatology of the "bomb." *Mon. Wea. Rev.*, **108**(10), 1 589–1 606, https://doi.org/10.1175/1520-0493(1980)108<1589:SDCOT>2.0.CO;2.

Seiler, C., and F. W. Zwiers, 2016: How will climate change affect explosive cyclones in the extratropics of the Northern Hemisphere? *Climate Dyn.*, **46**(11–12), 3 633–3 644, https://doi.org/10.1007/s00382-015-2791-y.

Sinclair, V. A., M. Rantanen, P. Haapanala, J. Räisänen, and H. Järvinen, 2020: The characteristics and structure of extra-tropical cyclones in a warmer climate. *Weather and Climate Dynamics*, **1**(1), 1–25, https://doi.org/10.5194/wcd-1-1-2020.

Taylor, K. E., R. J. Stouffer, and G. A. Meehl, 2012: An overview of CMIP5 and the experiment design. *Bull. Am. Meteorol. Soc.*, **93**(4), 485-498, https://doi.org/10.1175/BAMS-D-11-00094.1

Trenberth, K. E., and J. W. Hurrell, 1994: Decadal atmosphere-ocean variations in the Pacific. *Climate Dyn.*, **9**, 303–319, https://doi.org/10.1007/BF00204745.

Tilinina, N., S. K. Gulev, I. Rudeva, and P. Koltermann, 2013: Comparing cyclone life cycle characteristics and their interannual variability in different reanalyses. *J. Climate*, **26**(17), 6 419–6 438, https://doi.org/10.1175/JCLI-D-12-00777.1.

Wang, P. X., J. X. L. Wang, H. Zhi, Y. K. Wang, and X. J. Sun, 2012: Circulation indices of the Aleutian low pressure system: Definitions and relationships to climate anomalies in the northern hemisphere. *Adv. Atmos. Sci.*, **29**(5), 1 111–1 118, https://doi.org/10.1007/s00376-012-1196-7.

Yoshida, A., and Y. Asuma, 2004: Structures and environment of explosively developing extratropical cyclones in the northwestern Pacific region. *Mon. Wea. Rev.*, **132**(5), 1 121–1 142, https://doi.org/10.1175/1520-0493(2004)132<1121:SAEOED>2.0.CO;2.

Zhang, R. H., and S. Levitus, 1997: Structure and cycle of decadal variability of upper-ocean temperature in the North Pacific. *J. Climate*, **10**(4), 710–727, https://doi.org/10.1175/1520-0442(1997)010<0710:SACODV>2.0.CO;2.

Zhang, R. H., L. M. Rothstein, and A. J. Busalacchi, 1998: Origin of upper-ocean warming and El Niño change on decadal scales in the tropical Pacific Ocean. *Nature*, **391**, 879–883, https://doi.org/10.1038/36081.

Zhang, R. H., L. M. Rothstein, and A. J. Busalacchi, 1999: Interannual and decadal variability of the subsurface thermal structure in the Pacific Ocean: 1961-90. *Climate Dyn.*, **15**, 703–717, https://doi.org/10.1007/s003820050311.

Zhang, S. Q., G. Fu, C. G. Lu, and J. W. Liu, 2017: Characteristics of explosive cyclones over the Northern Pacific. *J. Appl. Meteor. Climatol.*, **56**(12), 3 187–3 210, https://doi.org/10.1175/JAMC-D-16-0330.1.

Zheng, Y. Q., S. F. Chen, W. Chen, R. G. Wu, Z. B. Wang, B. Yu, P. Hu, and J. Piao, 2024: The role of the Aleutian Low in the relationship between spring Pacific meridional mode and following ENSO. *J. Climate*, **37**(11), 3 249–3 268, https://doi.org/10.1175/jcli-d-23-0440.1.